Rare renal well-differentiated neuroendocrine tumors: clinical and imaging characteristics in a series of three cases

Rui Zeng[1,2]^, Liu Xu[3], Jianhua Wang[1], Lufei Jin[3], Zhihao Ren[3], Kaiwei Xu[3], Lu Hong[3], Yi Chen[4], Xiaohan Shen[5], Wenying Yu[5]

[1]Department of Radiology, The First Affiliated Hospital of Xiamen University, Xiamen, China; [2]Department of Urology, Mengchao Hepatobiliary Hospital of Fujian Medical University, Fuzhou, China; [3]Department of Radiology, The First Affiliated Hospital of Ningbo University, Ningbo, China; [4]Department of Radiology, Ningbo Medical Centre Li Huili Hospital, Ningbo Medical Center, Ningbo, China; [5]Ningbo Diagnostic Pathology Center, Ningbo, China

Correspondence to: Jianhua Wang, MD. Department of Radiology, The First Affiliated Hospital of Xiamen University, 55 Zhenhai Road, Siming District, Xiamen 361000, China. Email: wangjianhua@nbu.edu.cn.

Introduction

Neuroendocrine tumors (NETs) are uncommon neoplasms that exhibit notable neuroendocrine and neural differentiation phenotypes. These tumors are believed to arise from neuroendocrine cells distributed throughout the body. Primary renal well-differentiated neuroendocrine tumors (PRNTs), previously referred to as carcinoid tumors, represent an exceedingly rare subtype of renal tumors, with an incidence of only 0.13 per 1 million individuals (1,2).

In 2016, the renal tumor subcommittee reclassified PRNTs under the endocrine tumors category, which also includes small-cell neuroendocrine carcinomas, large-cell neuroendocrine carcinomas, and paragangliomas (3). This classification was reaffirmed in 2022 (4). The term carcinoid is no longer used. The current knowledge of this disease is primarily based on case reports, small series, and pooled studies. The study by Nguyen *et al.* in 2021 examined 166 cases from the Surveillance, Epidemiology, and End Results (SEER) database for the years spanning 1973 to 2014 and reported a 5-year survival rate of approximately 50%, which was significantly lower than that of other types of renal cancer (5). Nephrectomy with lymph node dissection is considered the standard treatment for localized PRNTs, which differs from other types of renal cancer. Therefore, preoperative diagnosis of PRNTs holds

significant importance.

The diagnostic methods for NETs include computed tomography (CT) and octreotide scans. However, no specific radiographic features for PRNTs have thus far been reported. Octreotide scintigraphy has limited utility in PRNTs due to the normal renal uptake of tracer material, which can obscure suspicious lesions (6). In contrast, magnetic resonance imaging (MRI) offers a more comprehensive imaging modality for the differential diagnosis of renal tumors. In this report, we present three cases of PRNTs treated at the First Affiliated Hospital of Ningbo University and summarize their CT and MRI characteristics, aiming to enhance our understanding of PRNTs.

Case presentation

Case 1

In June 2014, a 60-year-old female patient was admitted to the outpatient department with a chief complaint of persistent right lumbar back pain for 1 year. Upon physical examination, right lumbar back pain was the only notable finding. The patient did not report any significant past medical history or a family history of tumors. Routine laboratory tests, including complete blood count, urinalysis, and tumor markers [alpha fetoprotein (AFP), carbohydrate
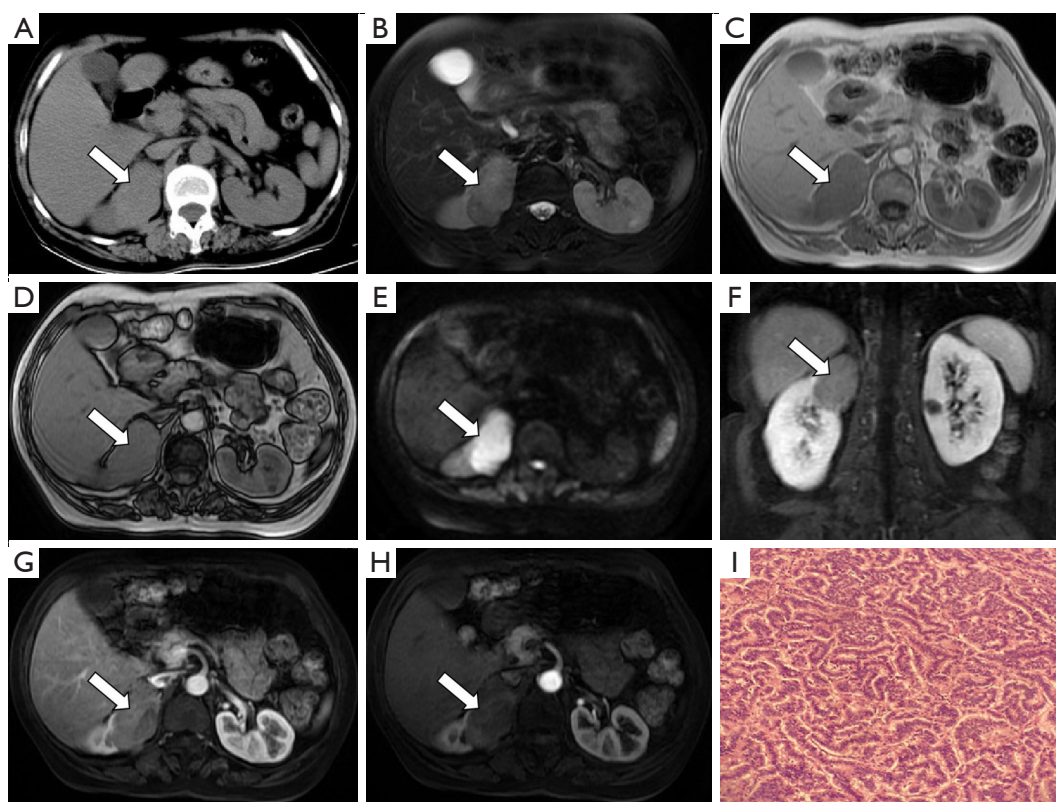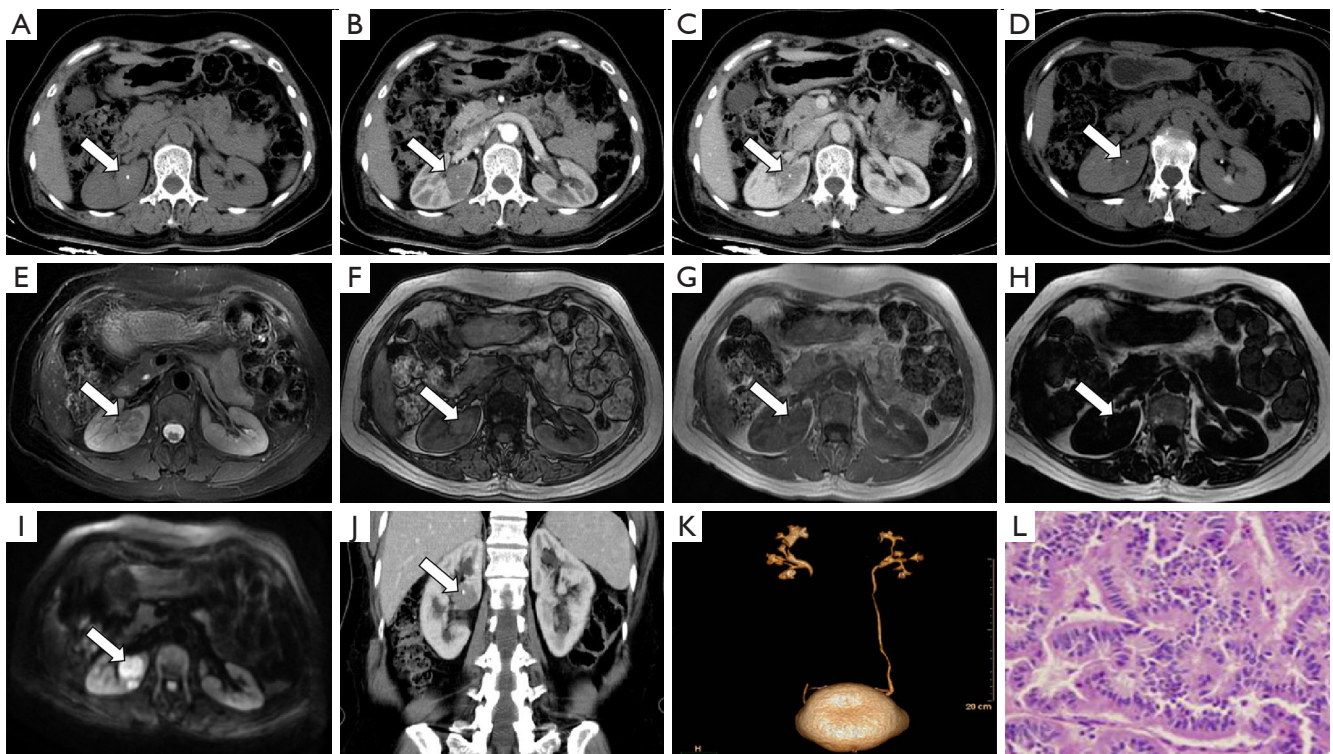
Figure 1 Preoperative renal pathology photographs and CT and MRI scans were obtained for case 1 (the white arrows indicate the neoplasm). (A) The plain CT scan demonstrated a slightly high-density (35 Hounsfield units) oval mass located in the upper pole of the right kidney. (B) On T2-weighted MRI, the mass exhibited slight hypointensity with nonuniform internal signal intensity. (C,D) MRI images revealed no signal decrease on the out-of-phase images compared to the in-phase images. (E) Diffusion-weighted imaging indicated restricted diffusion within the tumor. (F-H) Contrast-enhanced MRI showed slightly heterogeneous enhancement within the tumor. (I) Microscopic examination of the tumor tissue revealed clusters of closely arranged tumor cells with enlarged nuclei, hyperchromasia, finely granular chromatin, and inconspicuous nucleoli (hematoxylin and eosin staining, 200×). CT, computed tomography; MRI, magnetic resonance imaging.

antigen (CA) 19-9, and carcinoembryonic antigen (CEA)], yielded normal results. A plain CT scan revealed a well-defined, solid mass measuring 5.2 cm × 4.4 cm in size in the upper pole of the right kidney. The tumor appeared slightly hyperdense with a Hounsfield unit (HU) value of 35 (*Figure 1A*). The tumor protruded from the renal surface and was located close to the adrenal gland. MRI showed that the lesion was predominantly isointense on T1-weighted images and slightly hypointense on T2-weighted images (*Figure 1B*). Out-of-phase MRI demonstrated no signal loss compared to in-phase MRI (*Figure 1C,1D*). Diffusion-weighted imaging (DWI) revealed restricted diffusion within the tumor (*Figure 1E*). During the delayed phase of contrast enhancement, the tumor exhibited mild enhancement, which was lower

than that of the adjacent renal parenchyma. The lesion displayed heterogeneous signals, with punctate or flaky areas of lower signal intensity (*Figure 1F-1H*). This tumor was staged as T1bN0M0. The patient underwent radical right nephrectomy and adrenalectomy to remove the tumor in the upper pole of the right kidney, and no perioperative complications were encountered. Gross examination revealed a yellow or brown cut surface of the tumor. Pathological examination revealed closely arranged clumps or trabeculae of tumor cells. The tumor cells exhibited small size and a round or spindle-shaped morphology, demonstrating well-differentiated features with scant cytoplasm, slight atypia, and indistinct cell boundaries (*Figure 1I*). The nuclei displayed finely granular chromatin with inconspicuous nucleoli, and mitotic figures

1202

Zeng et al. Imaging characteristics of renal NETs

Figure 2 Preoperative renal pathology photographs and CT and MRI scans were obtained for case 2 (the white arrows indicate the neoplasm). The CT scan revealed a circular nodule lesion with soft tissue density in the right kidney, specifically in the middle pole. (A) The plain scan exhibited a CT value of approximately 45 HU, with evident calcification inside the lesion. (B-D) Dynamic contrast CT enhancement demonstrated mild enhancement (49 HU) in the cortical and parenchymal phases and decreased enhancement (43 HU) in the delayed phase. (E) On T2-weighted MRI, the mass appeared slightly hypointense. (F,G) Out-of-phase MRI signals did not show a decreased signal compared to the in-phase MRI images. (H) No obvious fat composition was observed within the tumor. (I) Diffusion-weighted imaging indicated restricted diffusion within the tumor. (J) A reconstructed coronal CT image demonstrated a clear perirenal fat space, indicating no invasion of the perinephric fat tissue. (K) CT urography revealed no hydronephrosis. (L) Microscopic examination of the tumor tissue revealed nests or trabeculae of tumor cells, with some arranged in an acinar pattern (hematoxylin and eosin staining, 400×). The tumor cells exhibited round or spindle-shaped morphology, poor differentiation, and marked cellular atypia. The nuclear chromatin appeared finely granular, and nucleoli were either absent or inconspicuous. CT, computed tomography; MRI, magnetic resonance imaging; HU, Hounsfield unit.

were rare. Immunohistochemical analysis demonstrated positive staining for synaptophysin (Syn), chromogranin A (CgA), CD56, and Ki-67 (40%), confirming the diagnosis of PRNT. The patient did not receive any adjuvant therapy such as chemotherapy or immunotherapy. No recurrence was observed at the most recent follow-up in November 2022 (100 months post-surgery).

Case 2

A 47-year-old female patient was admitted to the hospital with a complaint of right back pain after engaging in

physical activity for 4 weeks in April 2016. No other abnormalities were reported. This patient had no significant medical history or family history of tumors. Hemoglobin levels were slightly decreased (98 g/L). Other laboratory examinations, including complete blood count, urinalysis, and tumor markers (AFP, CA15-3, CA19-9, and CEA), were within normal limits. A CT scan revealed a circular nodular lesion measuring approximately 2.9 cm × 3.5 cm in size in the midpole of the right kidney. The lesion appeared isodense (45 HU) on a plain CT scan, with focal calcifications (*Figure 2A*). Dynamic contrast enhancement showed mild enhancement during the cortical (49 HU) and

parenchymal (56 HU) phases and decreased enhancement during the delayed phase (43 HU) (*Figure 2B-2D*). Abdominal MRI revealed a well-defined oval lesion in the midpole of the kidney, exhibiting similar imaging characteristics to those of case 1, with isointense signals on T1-weighted images and slight hypointensity on T2-weighted images (*Figure 2E*). Out-of-phase MRI did not demonstrate signal loss (*Figure 2F,2G*), and no obvious fat composition was observed within the tumor (*Figure 2H*). DWI showed restricted diffusion within the tumor (*Figure 2I*). Reconstructed coronal and sagittal CT images demonstrated a sharply demarcated lesion (*Figure 2J*). CT urography demonstrated that the tumor was close to the renal pelvis without evidence of hydronephrosis (*Figure 2K*). There was no evidence of tumor thrombus in the renal vein, regional lymph nodes, or distant metastases. The tumor was classified as T1aN0M0 according to the staging system. The patient underwent radical right nephrectomy due to the unfavorable location of the tumor. No perioperative complications were noted. Pathological examination revealed a tumor size of approximately 3.5 cm × 3 cm × 3 cm in size. The surgical margins were negative, and no invasion of the renal capsule or pelvis was observed. The cut surface displayed areas of necrosis and appeared brown in color. The neoplastic cells were arranged in nests, trabeculae, and acinar patterns, with occasional papillary structures (*Figure 2L*). The tumor cells exhibited small size, round, or spindle-shaped morphology, with well-differentiated features, scant cytoplasm, indistinct cell boundaries, and slight atypia. The nuclear chromatin was finely granular, and nucleoli were absent or inconspicuous. Rare mitotic figures were observed. Immunohistochemical analysis showed positive staining for Syn and CD56, while CgA and Ki-67 (1%) were negative. Pathological and immunohistochemical analyses confirmed the diagnosis of PRNT. No adjuvant therapy, such as chemotherapy or immunotherapy, was administered. No recurrence or metastasis was detected at the last follow-up in October 2022, 78 months after surgery.
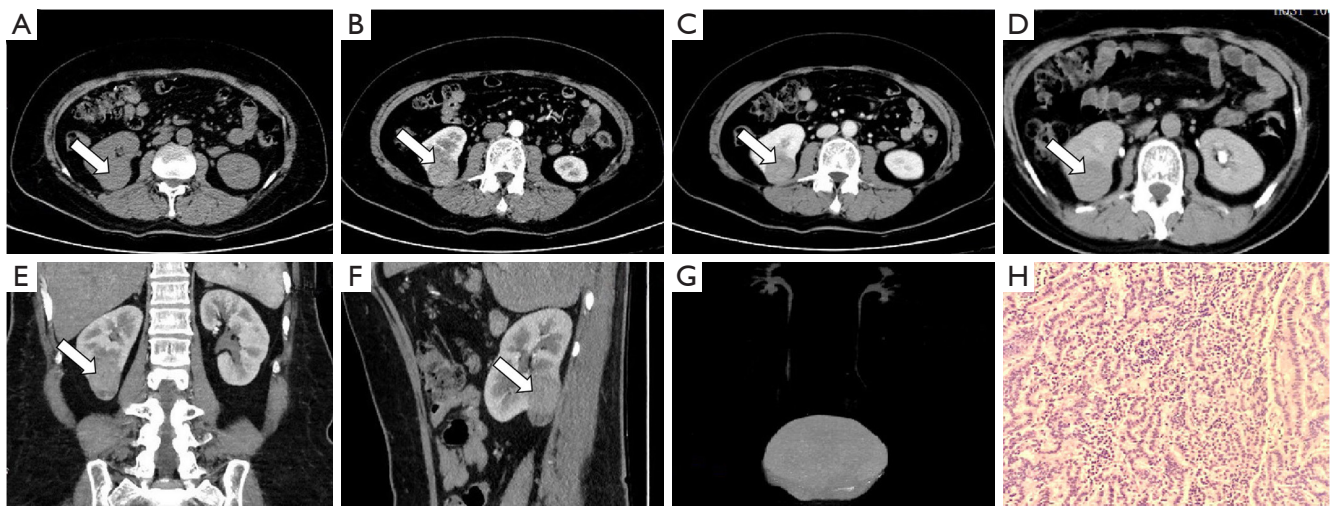
Case 3

A 55-year-old woman was admitted to the First Affiliated Hospital of Ningbo University after a right renal space-occupying lesion was incidentally discovered during a regular physical examination in January 2019. The patient did not report any discomfort. The patient had no noteworthy medical history or family history of tumors. Laboratory findings revealed increased levels of total bilirubin (23.5 μmol/L) and indirect bilirubin (19.6 μmol/L), with a slight decrease in albumin (34 g/L). Tumor markers (AFP, CA19-9, and CEA) were within normal limits. A CT scan revealed an exophytic circular tumor measuring approximately 2.7 cm × 3.4 cm in size in the lower part of the right kidney. The tumor appeared isodense (49 HU) on the plain scan, with mild enhancement during the cortical (76 HU) and parenchymal (85 HU) phases and decreased enhancement during the delayed phase (64 HU) (*Figure 3A-3D*). Reconstructed coronal and sagittal CT images demonstrated a sharply demarcated lesion (*Figure 3E,3F*). No evidence of tumor thrombus, regional lymph node metastasis, or distant metastasis was found. CT urography revealed no hydronephrosis (*Figure 3G*). Due to the tumor being staged as T1aN0M0, the patient underwent nephron-sparing radical nephrectomy, and no perioperative complications occurred. Gross examination of the tumor revealed yellow and brown cut surfaces. Microscopically, the tumor cells exhibited diffuse growth with few areas of local necrosis. The tumor cells displayed round or fusiform shapes with minimal atypia. The nuclei were enlarged and hyperchromatic, with fine granular chromatin, and rarely showed nuclear division (*Figure 3H*). Immunohistochemical analysis showed positive staining for Syn and CD56, while CgA and Ki-67 (3%) were negative. Pathological and immunohistochemical analyses confirmed the diagnosis of PRNT. The patient did not receive any adjuvant therapy, such as chemotherapy or immunotherapy, and no recurrence or metastasis was observed at the final follow-up in August 2022, 43 months after surgery.

All procedures performed in this study were in accordance with the ethical standards of the Medical Ethics Committee of The First Affiliated Hospital of Ningbo University and with the Helsinki Declaration (as revised in 2013). Written informed consent was obtained from the patients for publication of the case report and accompanying images. A copy of the written consent is available for review by the editorial office of this journal.

Discussion

NETs originate from neuroendocrine cells that are widely distributed throughout the body. Approximately 90% of NETs arise in the digestive or respiratory tracts (7). McGarrah *et al.* conducted a review of the SEER database and estimated that the incidence of PRNTs is exceptionally low, at only 0.13 per million individuals (2). PRNTs are considered extremely rare due to the absence of neuroendocrine cells in the renal tissue (8). The histogenesis of PRNTs remains

Figure 3 Preoperative pathology photographs and renal CT scans were obtained for case 3 (the white arrows indicate the neoplasm). (A) A plain CT scan revealed an oval mass with isodensity located at the lower pole of the right kidney, exhibiting a CT value of approximately 49 Hounsfield units. (B-D) On dynamic contrast-enhanced CT, the tumor displayed moderate enhancement (76 HU) in the cortical phase and parenchymal phase (85 HU), with decreased enhancement (64 HU) in the delayed phase. (E,F) Reconstructed coronal and sagittal CT images demonstrated a sharply demarcated lesion. (G) CT urography revealed no hydronephrosis. (H) Microscopic examination of the tumor tissue revealed diffuse growth and significant atypia of the tumor cells (hematoxylin and eosin staining, 20×). The nuclei appeared enlarged and hyperchromatic, with finely granular chromatin. Nuclear divisions were visible, and no significant staining of the nucleoli was observed. CT, computed tomography; MRI, magnetic resonance imaging; HU, Hounsfield unit.

uncertain, and the hypothesis that PRNTs arise directly from neuroendocrine cells in the renal pelvic urothelium is not widely accepted. There have been few reports of NETs arising in the renal pelvis and extending into the kidney, which are histologically and anatomically different from PRNTs. The relative risk of PRNTs in a horseshoe kidney compared to a nonhorseshoe kidney is approximately 62–82 times higher (9,10). This high association is likely due to teratogenic events involving the abnormal migration of posterior nephrogenic cells during embryogenesis, resulting in the formation of the isthmus of horseshoe kidneys (9). These neural crest tissues become entrapped within the developing kidney, and the fact that all horseshoe kidney-derived carcinoids are primarily located in the vicinity of the isthmus strongly supports this theory (11). However, the marker for developing metanephric tissue, PAX8, is negative in PRNTs, supporting a nonnephrogenic origin (10). Only approximately 12.8% of patients with renal neuroendocrine carcinomas have neuroendocrine syndromes (11), indicating a hindgut origin and the breakdown of secreted hormones in the liver before reaching the systemic circulation. Some reports on PRNTs have shown morphological and immunohistochemical features consistent with the hindgut

neuroendocrine phenotype (12), suggesting metastases from an occult NET elsewhere in the body. The most popular hypothesis, the totipotent cell hypothesis, states that PRNTs arise from primitive stem cells capable of neuroendocrine differentiation (13). However, direct evidence for this hypothesis is currently lacking.

PRNTs typically occur in patients aged 50–70 years (14). The average age of the three patients in this study was 55 years, which is consistent with previous reports. PRNTs tend to grow slowly and may remain asymptomatic for several years. Neuroendocrine syndromes are reported in only approximately 12.8% of patients with PRNTs (11), and none of the three patients in this study exhibited such syndromes. Other common symptoms include abdominal or loin pain, hematuria, constipation, frequent urination, fever, and weight loss (8). In this series, two out of the three patients reported right back pain. On imaging examination, PRNTs typically appear as unilateral, well-defined, solitary tumors. Histopathological examination is the mainstay for diagnosis. Grossly, PRNTs exhibit yellow or brown cut surfaces and may show areas of hemorrhage, calcification, or necrosis. Microscopically, PRNTs often display a trabecular, nested, or ribbon-like growth pattern with peripheral palisading.

Cytologically, the tumor cells exhibit fine granular "salt-and-pepper" chromatin patterns. Immunohistochemical markers such as CgA, Syn, neuron-specific enolase (NSE), and CD56 are valuable for diagnosing PRNTs (15). Surgical resection is the primary treatment for PRNTs, and several prognostic factors associated with a poor prognosis have been identified, including age at diagnosis greater than 40 years, severe initial symptoms, tumor diameter greater than 4 cm, tumor extension through the renal capsule, and presence of metastasis at the initial diagnosis (16).

Due to their rarity and diverse imaging features, the diagnosis of PRNTs using imaging techniques is challenging. Based on previous reports and the cases presented here, we summarize some major characteristics of PRNTs. PRNTs are well-differentiated neoplasms that are generally low-grade malignant cancers with slow growth rates. On CT scans, PRNTs typically appear as solid or cystic-solid, oval or lobulated, well-circumscribed masses. Hemorrhage is commonly observed, and approximately 25% of PRNTs may contain calcifications (17). In this study, case 2 exhibited calcification. According to research, calcification is linked to the less aggressive behavior of tumors, whereas hemorrhage and necrosis are associated with invasive growth and a poorer prognosis (11). This may partly explain why patients in this study experienced long-term survival without tumor recurrence. Another significant contributing factor is the early staging of the tumors. Lamb *et al.* reviewed 85 cases of PRNTs and found that 29% were hyperdense on CT scans, 55% were hypodense, and 15% were not specified. Among the enhanced cases, only 18% showed marked enhancement, and 14% showed mild enhancement (1). In the cases reported here, the tumors were solid masses without extensive necrosis or hemorrhage, demonstrating typical imaging characteristics of PRNTs. These characteristics, including mild enhancement in the cortex and renal parenchyma phases, along with decreased enhancement in the delayed phase, may be helpful in differentiating PRNTs from clear cell RCCs (ccRCCs). Typically, ccRCCs with a rich blood supply show significant heterogeneous enhancement and washout. The imaging features of PRNTs are indeterminate and overlap with those observed in papillary and chromophobe RCCs. The mild and decreased enhancement in PRNTs is likely related to poor blood supply. However, not only can the imaging features of PRNTs simulate papillary RCCs, but the occasional pathological appearance of PRNTs can also lead to misdiagnosis (18).

On noncontrast MRI, the PRNTs in this study cohort appeared isointense on T1-weighted images and slightly hypointense with heterogeneous internal signals on T2-weighted images. In contrast, ccRCCs typically show isointensity to hypointensity on T1-weighted images and hyperintensity on T2-weighted images, although larger ccRCCs may exhibit heterogeneous signal intensity due to necrosis and hemorrhage. The hypointense signals on T2-weighted images in PRNTs differ from those in ccRCCs. The signal characteristics of PRNTs, appearing isointense on T1-weighted images and slightly hypointense on T2-weighted images, are similar to those of papillary RCCs and chromophobe RCCs (19). Halefoglu *et al.* found that the presence of a predominantly papillary architecture in papillary RCCs, but not other factors such as ferritin, fresh blood, fibrosis, calcifications, or a high nucleus-to-cytoplasm ratio, correlated with a hypointense appearance on T2-weighted MRI (19). The trabecular, nested, or ribbon-like growth pattern with peripheral palisading in PRNTs may also correlate with a hypointense appearance on T2-weighted images, but further studies are needed to confirm this hypothesis. To our knowledge, no study has yet reported the sensitivity and specificity of tumors on T2-weighted images in differentiating PRNTs from ccRCCs. In our series, out-of-phase MRI signals showed no reduction compared to in-phase MRI due to the lack of fat content, and restricted diffusion was identified on DWI. These manifestations are not unique to PRNTs and can be present in various tumors. The tumors showed slight enhancement during the delayed phase of contrast-enhanced MRI, which was lower than that of the adjacent renal parenchyma. Additionally, the signals appeared nonuniform within the lesion, and punctate or flaky lower signals could be observed. These enhanced MRI characteristics were consistent with the features observed on enhanced CT scans, suggesting arterial insufficiency. Similarly, hypovascular or avascular lesions on renal angiography typically indicate deficient blood supply to the tumor parenchyma in PRNTs (6). The presence of evident hemorrhagic or necrotic areas in PRNTs indicates heterogeneity, making differential diagnosis difficult.

Octreotide scintigraphy is a commonly used method for diagnosing and staging gastrointestinal NETs. However, its applicability to PRNTs is limited due to a well-known limitation: the normal uptake of renal tracer can mask suspicious lesions (6). Therefore, octreotide scans could potentially be used as an additional tool for staging and monitoring metastatic PRNTs or for discovering NETs in other sites. The main limitation of this case report was the

lack of octreotide scintigraphy.

Conclusions

Currently, there are a limited number of reports focusing on the imaging characteristics of PRNTs. Thus, this study provides valuable insights into the understanding of PRNTs. Based on the existing literature and the analysis of three cases, PRNTs typically present as well-defined round masses with solid or cystic-solid composition on CT scans, and in some cases, they may show calcification. On MRI, PRNTs exhibit isointense signals on T1-weighted imaging (T1WI) and hypointensity on T2-weighted imaging (T2WI), resembling the signal characteristics observed in papillary and chromophobe RCCs, which helps to distinguish them from ccRCCs. Contrast-enhanced CT and MRI scans reveal mild enhancement during the cortex and renal parenchymal phases, which is followed by decreased enhancement in the delayed phase, suggesting compromised blood supply. This paper reports three cases of PRNTs, contributing to the clinical documentation of this rare disease. Particularly noteworthy is the fact that all cases presented as low-stage tumors with typical imaging features, free from confounding factors such as necrosis. These findings enhance the understanding of the radiological diagnosis of PRNTs.

Footnote

Conflicts of Interest: All authors have completed the ICMJE uniform disclosure form (available at https://qims.amegroups.com/article/view/10.21037/qims-23-1046/coif). R.Z. reports that this study was financially supported by the Natural Science Foundation of Fujian Province of China (No. 2021J011282). The other authors have no conflicts of interest to declare.

Ethical Statement: The authors are accountable for all aspects of the work in ensuring that questions related to the accuracy or integrity of any part of the work are appropriately investigated and resolved. All procedures performed in this study were in accordance with the ethical standards of the Medical Ethics Committee of The First Affiliated Hospital of Ningbo University and with the Helsinki Declaration (as revised in 2013). Written informed consent was obtained from the patients for publication of the case report and accompanying images. A copy of the written consent is available for review by the editorial office of this journal.

References

1. Lamb L, Shaban W. Primary renal carcinoid tumor: A radiologic review. Radiol Case Rep 2014;9:923.
2. McGarrah PW, Westin GFM, Hobday TJ, Scales JA, Ingimarsson JP, Leibovich BC, Halfdanarson TR. Renal Neuroendocrine Neoplasms: A Single-center Experience. Clin Genitourin Cancer 2020;18:e343-9.
3. Moch H, Cubilla AL, Humphrey PA, Reuter VE, Ulbright TM. The 2016 WHO Classification of Tumours of the Urinary System and Male Genital Organs-Part A: Renal, Penile, and Testicular Tumours. Eur Urol 2016;70:93-105.
4. Moch H, Amin MB, Berney DM, Compérat EM, Gill AJ, Hartmann A, Menon S, Raspollini MR, Rubin MA, Srigley JR, Hoon Tan P, Tickoo SK, Tsuzuki T, Turajlic S, Cree I, Netto GJ. The 2022 World Health Organization Classification of Tumours of the Urinary System and Male Genital Organs-Part A: Renal, Penile, and Testicular Tumours. Eur Urol 2022;82:458-68.
5. Nguyen AH, O'Leary MP, De Andrade JP, Ituarte PHG, Kessler J, Li D, Singh G, Chang S. Natural History of Renal Neuroendocrine Neoplasms: A NET by Any Other Name? Front Endocrinol (Lausanne) 2021;11:624251.
6. Lane BR, Jour G, Zhou M. Renal neuroendocrine tumors. Indian J Urol 2009;25:155-60.
7. Kim B, Kim HS, Moon KC. Primary renal well-differentiated neuroendocrine tumors: report of six cases

with an emphasis on the Ki-67 index and mitosis. Diagn Pathol 2019;14:12.

8. Chen CT, Hsieh SW, Hsieh TS. Case report: A case of primary renal carcinoid tumor. Urol Case Rep 2018;21:14-6.

9. Gupta S, Erickson LA. Primary Renal Well-Differentiated Neuroendocrine Tumor (Carcinoid) in a Horseshoe Kidney. Mayo Clin Proc 2021;96:1687-8.

10. Ungerer G, Steward JE, Akgul M, Cheng L, Sundaram CP. Clinical Considerations and Prognosis of Well-Differentiated Neuroendocrine Tumor Occurring Within a Renal Teratoma-A Case Series. Clin Genitourin Cancer 2021;19:e72-7.

11. Romero FR, Rais-Bahrami S, Permpongkosol S, Fine SW, Kohanim S, Jarrett TW. Primary carcinoid tumors of the kidney. J Urol 2006;176:2359-66.

12. Huettner PC, Bird DJ, Chang YC, Seiler MW. Carcinoid tumor of the kidney with morphologic and immunohistochemical profile of a hindgut endocrine tumor: report of a case. Ultrastruct Pathol 1991;15:655-61.

13. Deacon MJ, Harvey H, Shah C, Khan A. A Rare Case of a Large Primary Renal Neuroendocrine Tumour: A Case Report and Brief Review of Literature. Cureus 2021;13:e19743.

14. Amin M, Trikalinos N, Chatterjee D. Single institutional experience on primary neuroendocrine neoplasms of the kidney: a rare distinct entity. Hum Pathol 2021;114:36-43.

15. Jiang H, Zhang H. Clinical and Pathological Features of Primary Renal Well-Differentiated Neuroendocrine Tumor. Onco Targets Ther 2022;15:587-96.

16. Pivovarcikova K, Agaimy A, Martinek P, Alaghehbandan R, Perez-Montiel D, Alvarado-Cabrero I, Rogala J, Kuroda N, Rychly B, Gasparov S, Michalova K, Michal M, Hora M, Pitra T, Tuckova I, Laciok S, Mareckova J, Hes O. Primary renal well-differentiated neuroendocrine tumour (carcinoid): next-generation sequencing study of 11 cases. Histopathology 2019;75:104-17.

17. Chen Y, Shu Y, He L, Wu K. Primary renal carcinoid tumors: Three case reports. Medicine (Baltimore) 2021;100:e24714.

18. Dempsey PJ, O'Connell MJ, Bolster F. Solitary late metastasis of primary renal cell carcinoid tumor to the extraocular muscles imaged with indium-111 octreotide. World J Nucl Med 2021;20:99-101.

19. Halefoglu AM, Ozagari AA. Comparison of cortico-medullary phase contrast-enhanced MDCT and T2-weighted MR imaging in the histological subtype differentiation of renal cell carcinoma: radiology-pathology correlation. Pol J Radiol 2021;86:e583-93.